IEEE Access
Multidisciplinary ⋮ Rapid Review ⋮ Open Access Journal

Received January 4, 2022, accepted January 17, 2022, date of publication January 19, 2022, date of current version January 28, 2022.

Digital Object Identifier 10.1109/ACCESS.2022.3144836

Many-Objective Adaptive Fuzzy With Sliding Mode Control for a Class of Switching Power Converters Using Global Optimization

CHENG-LUN CHEN, (Member, IEEE)
Department of Electrical Engineering, National Chung Hsing University, Taichung 40227, Taiwan
e-mail: chenc@dragon.nchu.edu.tw

ABSTRACT Control of the power converters in renewable energy systems for stability and efficiency poses a technical challenge due to the intermittency of energy produced and inherent nonlinear dynamics. This paper presents a parametric optimization framework amid the synthesis of an adaptive fuzzy with sliding mode controller for a class of switching power converters suited for renewable energy systems. Four performance metrics essential to the practical needs are suggested. The potential design parameters of the controller are determined, and their influences on the performance metrics are studied and validated. A many-objective optimization problem is formulated accordingly, and a computational platform based on MATLAB/Simulink environment is established to solve the problem. Two multi-objective global search algorithms, i.e., particle swarm and bat optimization, are employed to obtain a set of Pareto optimal controllers, which noticeably enhance the performance metrics of the control system. An experimental platform with dSPACE controller board is utilized to further justify the simulation results. With those optimal controllers, the experimental results also demonstrate improvement of the performance.

INDEX TERMS Adaptive fuzzy control, bat optimization, many-objective optimization, particle swarm optimization, phase-shift pulse width modulation full bridge DC-DC converter, sliding mode control.

I. INTRODUCTION

All high-performance applications require a regulated and stable power supply, which in turn demands an intermediate voltage regulator circuit for energy conversion of high quality. Renewable energy systems, such as photovoltaic (PV), wind, and battery storage, have been allocated to the power grids and electric vehicles [1]–[3]. The intermittency of the energy, i.e., randomly varying output, generated by those systems deems power electronic converters a vital part of the systems [4]. Power converters, such as buck, boost, flyback, push-pull, and full bridge converters, have been developed to interface those energy sources for stable and efficient power conditioning and control [5]. It is worth notice that power intermittency and load variation would also drag the power converter off its designated operating point, and stimulate the nonlinear dynamics of the components within the converter [6]–[8]. Therefore, control of power converters in renewable energy applications is a technically challenging task.

Feedback controllers have been adopted to enhance the performance of the power converter from the aspects of transient and steady state responses [9]. Depending on the situation of application, simple or complex control algorithm may be considered. Simple controllers such as proportional-integral ones are easy to implement. However, they are usually designed for a certain operating point, thus is not resilient to input and parameter variation (i.e., lacks robustness). Robustness of these controllers have been improved for renewable energy applications, but achieving high performance is only possible when a thorough understanding of the converter in various operating points [10], [11] can be done. Control system design often comes across uncertainties. The uncertainties are due to disturbances, unknown parameters, nonlinear or unmodeled dynamics. To deal with nonlinear dynamics, feedback linearization is one common technique utilizing feedback to cancel part of or all the nonlinear terms. Adaptive feedback linearization can tackle both unknown parameters and nonlinear dynamics of certain structure

The associate editor coordinating the review of this manuscript and approving it for publication was Ton Duc Do.

TABLE 1. Optimization algorithms applied to DC-DC power converters.

Focus	Single/multiple objectives	Design parameters	Optimization algorithm	Robustness	Type of converter	Reference
Converter components	Single objective	Weight of heat sink, capacitor and inductor	Genetic algorithm	N/A	Two-phase interleaved bidirectional DC/DC Converter	[21]
		Turns ratio and switching frequency	Non-linear constrained optimization	N/A	Flyback dc–dc converter	[22]
		Switching frequency, duty ratio, coupling coefficient and the output voltage ripple	Particle swarm optimization	N/A	DC-DC boost converter	[23]
	Multiple objectives	Turn ratio, capacities and inductances	Active set algorithm	N/A	Phase-shift LLC series resonant converter	[24]
		Components of medium-frequency transformers	Genetic algorithm	N/A	LLC resonant converter	[25]
		Number of switches, drivers, and dc sources in each sub-multilevel	Particle swarm optimization	N/A	Cascade multilevel converter	[26]
Controller parameters	Single objective	Parameters of type-III controller	Particle swarm optimization	N/A	Interleaved boost converter	[27]
		Parameters of PI controller	Genetic algorithm	N/A	Phase-shift full bridge DC-DC converter	[28]
		Duty cycle of DC-DC boost converter	Particle swarm optimization	N/A	Boost DC-DC converter	[29]
		Duty cycles of converter switches	Bee colony optimization	N/A	Sheppard-Taylor converter	[30]
		Duty ratio of Cuk converter	Ant colony optimization	N/A	Cuk converter	[31]
		Parameters of fractional order PID controller	Artificial bee colony	transient disturbance	Zeta converter	[32]
		Parameters of feedback-type two-degree-of-freedom PID controller	Bat optimization	NA	Parallel bidirectional DC-DC converter.	[33]
	Multiple objectives	Parameters of adaptive fuzzy and sliding mode controller	Particle swarm optimization and bat optimization	disturbances and uncertain nonlinearities	Phase-shift full bridge DC-DC converter	This work

(e.g., which can be linearly parameterized). For more generic types of uncertainties, a revision, also known as adaptive fuzzy control, has been shown to be effective [12]–[14]. Adaptive fuzzy control uses radial basis function network (or fuzzy inference network) to approximate uncertainties of unknown parameters and structure [15]–[17]. Due to the network output being a linear combination of the outputs from the hidden nodes (i.e., radial basis or fuzzy membership function), the approximated uncertainties become linearly parameterized. Sliding mode control is robust to external disturbances and nonlinearities of no prior knowledge [18]–[20]. However, either the existence of unmodelled dynamics or improper controller design may result in high-frequency switching, i.e., issue of chattering. High-order sliding mode controllers may attenuate chattering. However, chattering caused by the unmodelled dynamics cannot be eliminated.

A few parameters of the controller can be decided by following the design procedure of a control algorithm, mostly related to stability or steady state convergence (the first concern of control system design). Other parameters of the controller, which have connection with alternative performance indicators, are mainly customizable. Analytical relationship between those performance indices and the customizable parameters is usually complex or not clear. Therefore, determination of those parameters poses a challenge when performance requirements apart from steady state response are also critical [21]. Optimization algorithms have been applied to power converters pursuing better conversion efficiency, lower switching losses, better time-domain response, and other objectives. Relevant previous works can be separated into two categories. The first category focuses on the design of converter components, e.g., transformer turn ratio, values of capacities, and inductances [21]–[26]. The second category concentrates on the design of controller parameters [27]–[33]. A detailed comparison is provided in Table 1. As can be seen, most works effectively improve the performance of the power converters, but no particular one outranks the others. Note also that most works only deal with single objective optimization. Neither do they consider the robustness of the control system.

Optimization algorithms have been applied to parameter design of the sliding mode controllers, e.g., gain and sliding surface [34]. Instead of trial and error, optimization approach can effectively reduce the effort and time for acquiring feasible controller parameters. Works on single objective optimization, e.g., minimizing operation cost or reliability, have been reported [23], [26], [35]. When more than one performance indices are deemed essential, resorting to multi- or many-objective optimization is sensible. Many-objective optimization refers to multi-objective

optimization problem containing large number of objectives, typically four or more. Two commonly used global optimization algorithms, suited for many-objective optimization, are particle swarm optimization and bat optimization [36]–[39]. Both are metaheuristic or swarm intelligence algorithms in terms of their mimicking collective behavior of ants, birds, fish, insects, or bats. Studies have shown that bat optimization algorithm solves constrained or unconstrained optimization problems with better robustness and efficiency. Not only can the algorithm increase the diversity of solutions in the population, it also has an automatic mechanism to balance exploration and exploitation during the search process.

This paper proposes a parametric optimization framework amid the synthesis of a robust adaptive fuzzy controller for a class of switching power converters. The open-loop system is a phase-shift pulse width modulation (PSPWM) full bridge DC-DC power converter, which is of practical interest due to features such as wide-range voltage output, high efficiency, etc. A comprehensive mathematical and the corresponding numerical model for this converter has been established in [40] and will be adopted in subsequent optimization and simulation. The closed-loop controller is an integration of adaptive fuzzy and sliding mode controls, and possesses advantageous traits from both design paradigms. The controller encompasses a set of customizable or design parameters, which will be adopted by the optimization problem to be formulated. Besides steady state error of the output voltage, alternative performance metrics, i.e., voltage ripple, peak load current, and transient efficiency, are also considered. To begin with, the negative or positive influence of the design parameters on performance metrics is studied. Conflicting performance metrics are also clarified. Next, a many-objective optimization problem is formulated. Subsequently, two global optimization methods, i.e., particle swarm optimization and bat optimization, are employed to numerically solve the problem and identify a set of Pareto optimal controller. Both simulation and experiment will be performed to validate the effectiveness of those optimal controllers. In summary, the main contributions of this work are as follows:

- A parametric optimization framework with multiple performance requirements is proposed, which is applicable to the synthesis of a robust adaptive fuzzy controller for a class of switching power converters.
- A many-objective optimization problem is formulated. Performance metrics of common practical needs are defined, and design parameters which influence the performance metrics are identified.
- Both computational and experimental platforms are established to automate and facilitate the acquirement of Pareto optimal controllers and the validation of the respective performance.
- The capability of the Pareto optimal controllers, in terms of the performance metrics, are justified both by simulation and experiment.

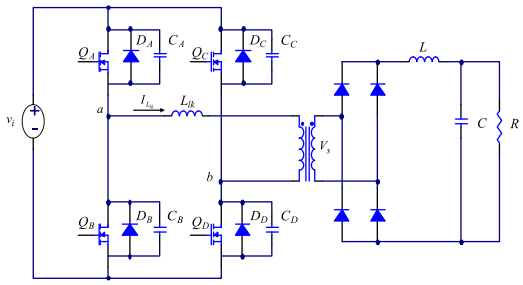

(a) Circuit diagram of a PSPWM full bridge DC-DC power converter.

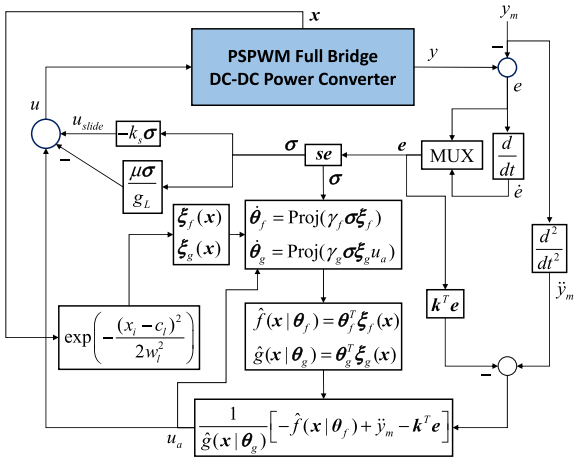

(b) Algorithmic configuration of adaptive fuzzy with sliding mode control.

FIGURE 1. The overall control system.

The rest of the paper is organized into Section II–VII. The operation and the state-space model for a PSPWM full bridge DC-DC power converter is reviewed in Section II, followed by design and synthesis of the adaptive fuzzy with sliding mode controller. Section III introduces performance metrics incorporated for the power converter and defines them quantitatively. The parameters of the adaptive fuzzy with sliding mode controller and their effect on the four indicators are studied. Section IV formulates the corresponding many-objective optimization problem. Two global optimization algorithms along with the concept of Pareto front for solving the problem are described in the context of this application. In Section V, a computing framework for parametric optimization of the controller is proposed. The control system with various sets of Pareto optimal parameters is numerically simulated, and the respective sets of performance metrics are compared. In Section VI, experimental setup is described and the results are demonstrated. Conclusion and future work are detailed in Section VII.

II. ADAPTIVE FUZZY WITH SLIDING MODE CONTROL SYSTEM

As illustrated in Fig. 1, the overall system has the structure of a PSPWM full bridge DC-DC power converter and an adaptive fuzzy with sliding mode controller. This section will summarize the operation and first-principle modeling of the converters, which is followed by design and synthesis of the controller.

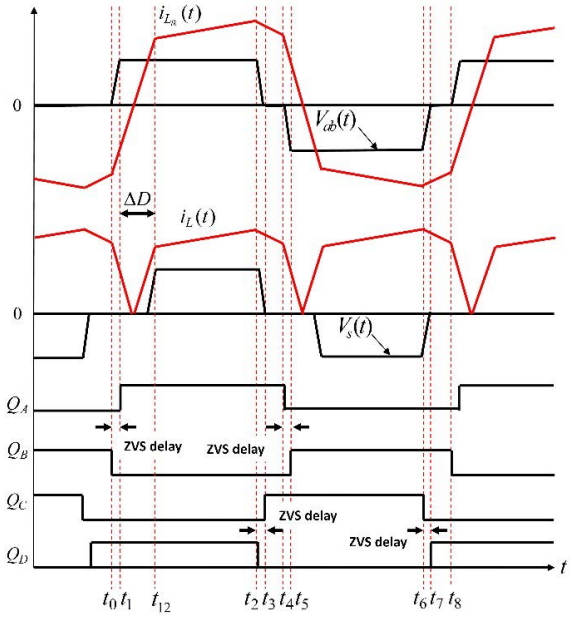

FIGURE 2. Operation waveforms and timing diagram of PSPWM full bridge DC-DC power converter.

PSPWM full bridge DC-DC power converters draw practical interest due to characteristics like wide-range voltage output, high efficiency, etc. This category of converters provides voltage translation as well as isolation from the line voltage since the circuit topology includes a transformer. A typical PSPWM full bridge DC-DC power converter consists of five key components, as shown in Fig. 1(a), which are metal oxide semiconductor field effect transistors (MOSFET) switches, PWM signal generator, leakage inductance, high frequency transformer, and rectification filter, from primary side to secondary side. With the help of leakage inductance L_{lk} and resonance capacitances (C_A, C_B, C_C, and C_D), the power converter accomplishes zero voltage soft switching (ZVS), achieving high efficiency power conversion.

The waveforms of primary current $i_{L_{lk}}$, secondary current i_L, voltage between point a and b of primary side V_{ab}, and secondary voltage V_s, as well the timing diagram for the four switches Q_A, Q_B, Q_C and Q_D of a PSPWM full bridge DC-DC converter, is illustrated in Fig. 2. Specifically, the system dynamics of the full bridge power converter can be divided into eight (or ten) regions, labeling from one to eight, where four of them are in positive half cycle: trailing leg transition region from t_0 to t_1, active region from t_1 to t_2 (this region actually contains one additional sub-region of duty cycle loss, i.e., t_1 to t_{12}), leading leg transition region from t_2 to t_3, and passive region from t_3 to t_4, and the other four regions are in negative half cycle, respectively.

A set of elaborate control-oriented state variable models comprising each operation interval were established [40]. The corresponding computational model is established using MATLAB/Simulink. The dynamics of the established model has been justified to be close to that of a conventional PSPWM full bridge DC-DC power converter in a laboratory environment. This computational model will be utilized for subsequent parametric optimization and verification.

From the perspective of control system design, utilization of elaborate computational model is advantageous and occasionally indispensable in various scenarios (e.g., reducing time and effort of design iteration, saving cost of experimentation). When it comes to controller synthesis, a sophisticated model is often too complex to be tackled with standard techniques. Hence, model reduction techniques are commonly employed to reduce the computational cost and storage requirement. The goal is to obtain a low dimensional model that encompasses the imperative dynamics of the sophisticated model. The 'neglected' dynamics can be addressed later on by adopting appropriate control paradigm.

Refer to the models established for the ten (including duty cycle loss) operation intervals [40]. Suppose that the extent of time is 1 for completing a cycle of operation (positive and negative half cycles). An averaging state-space model of the PSPWM full bridge DC-DC power converter can be formulated as

$$\begin{aligned} \dot{\boldsymbol{x}}(t) &= \boldsymbol{A}\boldsymbol{x}(t) + \boldsymbol{B}u(t), \\ y(t) &= \boldsymbol{C}\boldsymbol{x}(t), \end{aligned} \tag{1}$$

where $u(t)$ is the input voltage of the power converter $v_i(t)$, $y(t)$ is the output voltage of the power converter $v_o(t)$. With v_{C_A} the voltage across C_A, v_{C_B} the voltage across C_B, v_{C_C} the voltage across C_C, and v_{C_D} the voltage across C_D, the state $\boldsymbol{x}(t)$ is defined as

$$\boldsymbol{x}(t) = [i_{L_{lk}}(t) \;\; i_L(t) \;\; v_o(t) \;\; v_{C_A}(t) \;\; v_{C_B}(t) \;\; v_{C_C}(t) \;\; v_{C_D}(t)]^{\mathrm{T}}. \tag{2}$$

The matrices $\boldsymbol{A}$, $\boldsymbol{B}$ and $\boldsymbol{C}$ are defined in (3), as shown at the bottom of the next page, where L and C are inductance and capacitance of the rectification filter, R is load, and n is turn ratio of the transformer. Note that d_1, d_2, d_3, and d_4 are percentage durations with respect to four of the operation intervals (duration of the remaining one is $0.5 - d_1 - d_2 - d_3 - d_4$). Disregarding the uncontrollable and unobservable parts of the model, we obtain

$$\begin{bmatrix} \dot{i}_{\mathrm{L}} \\ \dot{v}_o \end{bmatrix} = \begin{bmatrix} 0 & \dfrac{2d_2 - 1}{n^2 L_{lk} + L} + \dfrac{-2d_2}{L} \\ 1/C & -1/RC \end{bmatrix} \begin{bmatrix} i_L \\ v_o \end{bmatrix} + \begin{bmatrix} 2\dfrac{-nd_1 + nd_3 + nd_4}{n^2 L_{lk} + L} \\ 0 \end{bmatrix} v_i. \tag{4}$$

Further simplification can be made by letting $d_1 = d_4$ (symmetry of operation) and $n^2 L_{lk} + L \cong L$ ($L \gg L_{lk}$), and setting $2d_3 = d$. We have

$$\begin{bmatrix} \dot{i}_L \\ \dot{v}_o \end{bmatrix} = \begin{bmatrix} 0 & -1/L \\ 1/C & -1/RC \end{bmatrix} \begin{bmatrix} i_L \\ v_o \end{bmatrix} + \begin{bmatrix} nd/L \\ 0 \end{bmatrix} v_i. \tag{5}$$

Equation (5) can also be obtained by neglecting the transition intervals and taking only the dynamics of active and passive regions into consideration. Choose the state $[x_1\ x_2]^T$ as $[i_L\ v_o]^T$, the input as d, and the direct output as v_o. We obtain

$$\begin{bmatrix}\dot{x}_1\\ \dot{x}_2\end{bmatrix}=\begin{bmatrix}0 & -1/L\\ 1/C & -1/RC\end{bmatrix}\begin{bmatrix}x_1\\ x_2\end{bmatrix}+\begin{bmatrix}nv_i/L\\ 0\end{bmatrix}u \quad \text{and} \quad y=x_2. \tag{6}$$

By input-output linearization, the output differential model subject to disturbance is

$$\begin{aligned}\ddot{y}&=f(\boldsymbol{x})+g(\boldsymbol{x})u+\eta(t,\boldsymbol{x})\\&=\left[\frac{-1}{RC^2}x_1+\left(\frac{1}{R^2C^2}-\frac{1}{LC}\right)x_2\right]+\left(\frac{nv_i}{LC}\right)u+\eta(t,\boldsymbol{x}),\end{aligned} \tag{7}$$

where the plant disturbance η is nonzero and assumed to be less than a positive constant d, i.e., $|\eta(t,\boldsymbol{x})|\le d$. In addition, $g(\boldsymbol{x})$ is assumed to have a positive lower bound, i.e., $g(\boldsymbol{x})\ge g_L>0$. Define the tracking error as $\boldsymbol{e}=[y-y_m\ \dot{y}-\dot{y}_m]^T=[e\ \dot{e}]^T$. Let $\boldsymbol{s}=[k_1\ 1]$ (with a design parameter) and $\sigma(\boldsymbol{e})=\boldsymbol{se}$. Then, $\{\boldsymbol{e}:\sigma(\boldsymbol{e})=0\}$ represents a sliding surface in the tracking error space. The objective is to construct a control input u so that $\lim_{t\to\infty}\boldsymbol{e}=0$. If $f(\boldsymbol{x})$ and $g(\boldsymbol{x})$ in (7) are certain and $\eta=0$, the control input can be specified as

$$u^*=\frac{1}{g}(-f-\mu\sigma+\ddot{y}_m-\boldsymbol{k}^T\boldsymbol{e}), \tag{8}$$

where $\mu>0$ and $\boldsymbol{k}=[0\ k_2]^T$ (with a design parameter). Let $V=\sigma^2/2$. We have

$$\begin{aligned}\dot{V}&=\sigma\dot{\sigma}=\sigma\boldsymbol{s}\dot{\boldsymbol{e}}=\sigma(\ddot{e}+s_1\dot{e})\\&=\sigma(\ddot{y}-\ddot{y}_m+\boldsymbol{k}^T\boldsymbol{e})=\sigma(f+gu-\ddot{y}_m+\boldsymbol{k}^T\boldsymbol{e}).\end{aligned} \tag{9}$$

Substituting the control law given by (8) yields $\dot{V}=-\mu\sigma^2$. Thus, the sliding surface $\{\sigma(\boldsymbol{e})=0\}$ is asymptotically attractive and the system restricted to the sliding surface can be made asymptotically stable with respect to the origin by an appropriate choice of the parameter k_1.

When $f(\boldsymbol{x})$ and $g(\boldsymbol{x})$ in (7) are uncertain and $\eta\neq0$, we may approximate both functions by

$$\hat{f}(\boldsymbol{x}|\boldsymbol{\theta}_f)=\boldsymbol{\theta}_f^T\boldsymbol{\xi}_f(\boldsymbol{x}) \text{ and } \hat{g}(\boldsymbol{x}|\boldsymbol{\theta}_g)=\boldsymbol{\theta}_g^T\boldsymbol{\xi}_g(\boldsymbol{x}), \tag{10}$$

where $\boldsymbol{\xi}_f(\boldsymbol{x})$ or $\boldsymbol{\xi}_g(\boldsymbol{x})$ is a set of radial basis function, $\boldsymbol{\theta}_f$ and $\boldsymbol{\theta}_g$ are adaptation parameters. Specifically,

$$\boldsymbol{\theta}_f=[\theta_{1f},\ldots,\theta_{Mf}]^T,\quad \boldsymbol{\theta}_g=[\theta_{1g},\ldots,\theta_{Mg}]^T, \tag{11}$$

$$\boldsymbol{\xi}_f(\boldsymbol{x})=[\xi_{1f}(\boldsymbol{x}),\ldots,\xi_{Mf}(\boldsymbol{x})]^T, \tag{12}$$

$$\boldsymbol{\xi}_g(\boldsymbol{x})=[\xi_{1g}(\boldsymbol{x}),\ldots,\xi_{Mg}(\boldsymbol{x})]^T, \tag{13}$$

where M is the number of fuzzy rules (or radial basis functions) and the elements of $\boldsymbol{\xi}_f(\boldsymbol{x})$ and $\boldsymbol{\xi}_g(\boldsymbol{x})$ can be described by

$$\xi_{l,f\text{ or }g}(\boldsymbol{x})=\frac{\prod_{i=1}^{2}\mu_{F_i^l}(x_i)}{\sum_{l=1}^{M}\prod_{i=1}^{2}\mu_{F_i^l}(x_i)},\quad l=1,\ldots,M \tag{14}$$

where $\mu_{F_i^l}(\cdot)$ is a Gaussian membership function. The optimal parameters are denoted by

$$\begin{cases}\boldsymbol{\theta}_f^*=\arg\min_{\boldsymbol{\theta}_f}[\sup_{\boldsymbol{x}\in R^2}\left|\hat{f}(\boldsymbol{x}|\boldsymbol{\theta}_f)-f(\boldsymbol{x})\right|],\\ \boldsymbol{\theta}_g^*=\arg\min_{\boldsymbol{\theta}_g}[\sup_{\boldsymbol{x}\in R^2}\left|\hat{g}(\boldsymbol{x}|\boldsymbol{\theta}_g)-g(\boldsymbol{x})\right|].\end{cases} \tag{15}$$

Assume that

$$\left|f(\boldsymbol{x})-\hat{f}(\boldsymbol{x}|\boldsymbol{\theta}_f^*)\right|\le d_f \quad \text{and} \quad \left|g(\boldsymbol{x})-\hat{g}(\boldsymbol{x}|\boldsymbol{\theta}_g^*)\right|\le d_g, \tag{16}$$

where $d_f>0$, $d_g>0$. Elements of $\boldsymbol{\theta}_f^*$ and $\boldsymbol{\theta}_g^*$ are constant and bounded as follows:

$$\theta_{Lfi}\le\theta_{fi}^*\le\theta_{fi}^U,\quad \theta_{Lgi}\le\theta_{gi}^*\le\theta_{gi}^U \text{ for } i=1\ldots M. \tag{17}$$

Define the parametric error of adaptation as

$$\boldsymbol{\phi}_f=\boldsymbol{\theta}_f-\boldsymbol{\theta}_f^* \quad \text{and } \boldsymbol{\phi}_g=\boldsymbol{\theta}_g-\boldsymbol{\theta}_g^*. \tag{18}$$

$$\boldsymbol{A}=\begin{bmatrix}0 & 0 & 0 & \frac{-n^2d_1}{n^2L_{lk}+L} & \frac{n^2d_1}{n^2L_{lk}+L} & \frac{n^2d_4}{n^2L_{lk}+L} & \frac{-n^2d_4}{n^2L_{lk}+L}\\ 0 & 0 & \frac{2d_2-1}{n^2L_{lk}+L}+\frac{-2d_2}{L} & \frac{nd_1}{n^2L_{lk}+L} & \frac{nd_1}{n^2L_{lk}+L} & \frac{-nd_4}{n^2L_{lk}+L} & \frac{-nd_4}{n^2L_{lk}+L}\\ 0 & \frac{1}{C} & \frac{-1}{RC} & 0 & 0 & 0 & 0\\ 2d_1/(C_A+C_B) & 0 & 0 & 0 & 0 & 0 & 0\\ -2d_1/(C_A+C_B) & 0 & 0 & 0 & 0 & 0 & 0\\ -2d_4/(C_C+C_D) & 0 & 0 & 0 & 0 & 0 & 0\\ 2d_4/(C_C+C_D) & 0 & 0 & 0 & 0 & 0 & 0\end{bmatrix},$$

$$\boldsymbol{B}=\left[0,2\frac{-nd_1+nd_3+nd_4}{n^2L_{lk}+L},0,0,0,0,0\right]^T,\quad \text{and } \boldsymbol{C}=[0,0,1,0,0,0,0]. \tag{3}$$

The adaptation law is specified as

$$\dot{\boldsymbol{\theta}}_f = \text{Proj}\left(\gamma_f \boldsymbol{\sigma} \boldsymbol{\xi}_f\right), \quad \dot{\boldsymbol{\theta}}_g = \text{Proj}\left(\gamma_g \boldsymbol{\sigma} \boldsymbol{\xi}_g u_a\right), \tag{19}$$

where γ_f and γ_g are positive design parameters. The projection operator is defined by

$$\dot{\theta}_i(t) = \text{Proj}\left(\alpha_i(t)\right) = \begin{cases} 0 & \text{if } \theta_i = \theta_{Li} \quad \text{and} \quad \alpha_i(t) < 0, \\ 0 & \text{if } \theta_i = \theta_i^U \quad \text{and} \quad \alpha_i(t) > 0, \\ \alpha_i(t) & \text{otherwise.} \end{cases} \tag{20}$$

The control law is specified as

$$\begin{cases} u = u_a - \dfrac{1}{g_L}\mu\sigma + u_{slide}, \\ u_a = \dfrac{1}{\hat{g}(\boldsymbol{x}|\boldsymbol{\theta}_g)}(-\hat{f}(\boldsymbol{x}|\boldsymbol{\theta}_f) + \ddot{y}_m - \boldsymbol{k}^T\boldsymbol{e}), \quad u_{slide} = -k_s\sigma, \end{cases} \tag{21}$$

with selection of k_s described in the proof of the subsequent theorem.

Theorem 1: The control law (21) along with parametric adaptation law (19). If u_{slide} satisfies

$$\begin{cases} \sigma\left(f - \ddot{y}_m + \boldsymbol{k}^T\boldsymbol{e} + gu_a + gu_{slide} + \eta\right) \le \gamma, \\ \sigma u_{slide} \le 0, \end{cases} \tag{22}$$

with $\gamma > 0$, we have the following:

1) $\sigma^2(t) \le e^{-2\mu t}\sigma^2(0) + \gamma/\mu$.

2) If $\eta = 0$ and there exists $\boldsymbol{\theta}_f^*$ and $\boldsymbol{\theta}_g^*$ such that $f(\boldsymbol{x}) = \boldsymbol{\theta}_f^{*T}\boldsymbol{\xi}_f$ and $g(\boldsymbol{x}) = \boldsymbol{\theta}_g^{*T}\boldsymbol{\xi}_g$, the origin of the $\left[\sigma \ \boldsymbol{\phi}_f \ \boldsymbol{\phi}_g\right]^T$-space is stable and hence $\sigma(t)$, $\boldsymbol{\phi}_f(t)$, and $\boldsymbol{\phi}_g(t)$ are bounded and $\lim_{t\to\infty} e(t) = 0$.

Proof: Let $V = \sigma^2/2$.

$$\begin{aligned} \dot{V} &= \sigma\dot{\sigma} = \sigma(f + gu + \eta - \ddot{y}_m + \boldsymbol{k}^T\boldsymbol{e}) \\ &= \sigma(f + gu_a - \frac{g}{g_L}\mu\sigma + gu_{slide} + \eta - \ddot{y}_m + \boldsymbol{k}^T\boldsymbol{e}) \\ &\le -\frac{g}{g_L}\mu\sigma^2 + \gamma \le -2\mu V + \gamma. \end{aligned} \tag{23}$$

$$V(t) \le e^{-2\mu t}V(0) + \frac{\gamma}{2\mu}(1 - e^{-2\mu t}) \le e^{-2\mu t}V(0) + \frac{\gamma}{2\mu}. \tag{24}$$

Let $V = \frac{1}{2}(\sigma^2 + \frac{1}{\gamma_f}\boldsymbol{\phi}_f^T\boldsymbol{\phi}_f + \frac{1}{\gamma_g}\boldsymbol{\phi}_g^T\boldsymbol{\phi}_g)$,

$$\begin{aligned} \dot{V} &= \sigma(-\frac{g}{g_L}\mu\sigma + f - \boldsymbol{\theta}_f^T\boldsymbol{\xi}_f + (g - \boldsymbol{\theta}_g^T\boldsymbol{\xi}_g)u_a \\ &\quad + gu_{slide}) + \frac{1}{\gamma_f}\boldsymbol{\phi}_f^T\dot{\boldsymbol{\phi}}_f + \frac{1}{\gamma_g}\boldsymbol{\phi}_g^T\dot{\boldsymbol{\phi}}_g \\ &= \sigma(f - \boldsymbol{\theta}_f^T\boldsymbol{\xi}_f + (g - \boldsymbol{\theta}_g^T\boldsymbol{\xi}_g)u_a + gu_{slide}) - \frac{g}{g_L}\mu\sigma^2 \\ &\quad + \boldsymbol{\phi}_f^T\frac{1}{\gamma_f}\text{Proj}(\gamma_f\sigma\boldsymbol{\xi}_f) + \boldsymbol{\phi}_g^T\frac{1}{\gamma_g}\text{Proj}(\gamma_g\sigma\boldsymbol{\xi}_g u_a) \\ &= -\frac{g}{g_L}\mu\sigma^2 + \sigma gu_{slide} - \boldsymbol{\phi}_f^T\boldsymbol{\xi}_f\sigma + \boldsymbol{\phi}_f^T\frac{1}{\gamma_f}\text{Proj}(\gamma_f\sigma\boldsymbol{\xi}_f) \\ &\quad - \boldsymbol{\phi}_g^T\boldsymbol{\xi}_g\sigma u_a + \boldsymbol{\phi}_g^T\frac{1}{\gamma_g}\text{Proj}(\gamma_g\sigma\boldsymbol{\xi}_g u_a) \\ &\le -\mu\sigma^2 + \sigma gu_{slide} \le -\mu\sigma^2. \end{aligned} \tag{25}$$

It follows that the system is stable and $\sigma(t)$, $\boldsymbol{\phi}_f(t)$, and $\boldsymbol{\phi}_g(t)$ are bounded.

Let $h_f \ge \|\boldsymbol{\xi}_f\| \left\|\boldsymbol{\theta}_f^U - \boldsymbol{\theta}_{Lf}\right\|$ and $h_g \ge \|\boldsymbol{\xi}_g\| \left\|\boldsymbol{\theta}_g^U - \boldsymbol{\theta}_{Lg}\right\| |u_a|$. When k_s is specified such that

$$k_s \ge \frac{1}{g_L}\left(\frac{d_f^2 + |u_a|^2 d_g^2}{2\gamma_1} + \frac{h_f^2}{4\gamma_2} + \frac{h_g^2}{4\gamma_3} + \frac{d^2}{4\gamma_4}\right), \tag{26}$$

we show that (22) is satisfied. Indeed, considering (26) and rearranging terms gives

$$\begin{aligned} &\sigma(f - \ddot{y}_m + \boldsymbol{k}^T\boldsymbol{e} + gu_a + gu_{slide} + \eta) \\ &\le \sigma(f - \boldsymbol{\theta}_f^{*T}\boldsymbol{\xi}_f - \frac{d_f^2\sigma}{2\gamma_1}) + \sigma((g - \boldsymbol{\theta}_g^{*T}\boldsymbol{\xi}_g)u_a - \frac{|u_a|^2 d_g^2\sigma}{2\gamma_1}) \\ &\quad - \sigma(\boldsymbol{\phi}_f^T\boldsymbol{\xi}_f + \frac{h_f^2\sigma}{4\gamma_2}) - \sigma(\boldsymbol{\phi}_g^T\boldsymbol{\xi}_g u_a + \frac{h_g^2\sigma}{4\gamma_3}) + \sigma(\eta - \frac{d^2\sigma}{4\gamma_4}). \end{aligned} \tag{27}$$

Completing the square yields

$$\begin{aligned} &\sigma(f - \ddot{y}_m + \boldsymbol{k}^T\boldsymbol{e} + gu_a + gu_{slide} + \eta) \\ &\le \left(\frac{f - \boldsymbol{\theta}_f^{*T}\boldsymbol{\xi}_f}{\sqrt{2}\, d_f \Big/ \sqrt{\gamma_1}}\right)^2 + \left(\frac{(g - \boldsymbol{\theta}_g^{*T}\boldsymbol{\xi}_g)u_a}{\sqrt{2}\,|u_a|\, d_g \Big/ \sqrt{\gamma_1}}\right)^2 \\ &\quad + \left(\frac{\boldsymbol{\phi}_f^T\boldsymbol{\xi}_f}{h_f^2 \Big/ \sqrt{\gamma_2}}\right)^2 + \left(\frac{\boldsymbol{\phi}_g^T\boldsymbol{\xi}_g u_a}{h_g^2 \Big/ \sqrt{\gamma_3}}\right)^2 + \left(\frac{\eta}{d \Big/ \sqrt{\gamma_4}}\right)^2 \\ &\le \frac{1}{2}\gamma_1 + \frac{1}{2}\gamma_1 + \gamma_2 + \gamma_3 + \gamma_4 = \gamma. \end{aligned} \tag{28}$$

Therefore, (22) holds. □

III. PERFORMANCE METRICS AND DESIGN PARAMETERS

An understanding of the features and parameters is crucial for choosing applicable DC-DC power converters. Typical "static" parameters are input voltage range, output voltage range, and maximum required output current. Typical "dynamic" parameters are efficiency, output voltage ripples, and load transient regulation. There are also various practical aspects being regularly taken into consideration: EMI, size, input voltage ripple, operating temperature, output ripple frequency, failure rate, etc. When reviewing the features and parameters of converters, it is important to understand the different trade-offs between performance metrics. This helps determine realistic expectations for the converter that best fits the application. In this section, performance metrics incorporated for PSPWM full bridge DC-DC power converter are introduced and quantitatively defined. The potential design parameters of the adaptive fuzzy with sliding mode controller and their effect on the four indicators are studied.

A. PERFORMANCE METRICS

Four metrics are incorporated in this paper for performance evaluation of the PSPWM full bridge DC-DC power converter: root mean square error (RMSE), voltage ripple, switching peak load current, and transient conversion efficiency. Optimize these four performance indicators at the

same time is challenging due to some of them being conflicting indices (as will be shown in subsequent study). In the following, we explain the practical meaning of the four metrics and provide their mathematical definition.

The first metric is RMSE defined by

$$\text{RMSE} = \sqrt{\frac{1}{N}\sum_{k=1}^{N}\left[e\left(k\right)^2\right]} \text{ and } e(k) = V_{ref}(k) - V_o(k), \tag{29}$$

where k indexes the ordered samples, N is the number of samples, $e(k)$ is the difference between reference voltage $V_{ref}(k)$ and output voltage $V_o(k)$. For this study, both transient and steady-state responses will be accounted for this metric. Hence, it is sensitive to large errors in a set of measurements and well reflects the quality of transient dynamics of the converter. The second metric is voltage ripple V_{ripple}, which assesses the quality of steady-state dynamics of the converter. It is defined by

$$V_{ripple} = \frac{1}{2}\left[\max_k V_o(k) - \min_k V_o(k)\right]. \tag{30}$$

For static reference voltage, voltage ripple can also be evaluated by

$$\max_k V_o(k) - V_{ref}. \tag{31}$$

The third metric is switching peak load current $i_{L,\max}$, which is generated as the power converter is switched on. It induces a sudden component stress and may fasten the degradation of the converter. The switching peak load current is defined by

$$i_{L,\max} = \max_k \left(i_L\left(k\right)\right), \tag{32}$$

where $i_L(k)$ is the load current. The fourth metric is transient efficiency E_f. Different from the conventional definition, the transient efficiency focuses on the transient dynamics of the converter between switching on and reaching steady state. The transient efficiency is defined as

$$E_f = \frac{V_{o(rms)}I_{o(rms)}}{V_{i(rms)}I_{i(rms)}} \times 100\%, \tag{33}$$

where $V_{o(rms)}$, $V_{i(rms)}$, $I_{o(rms)}$, and $I_{i(rms)}$ represent the effective (RMS) values of the output voltage, input voltage, output current, and input current, respectively.

B. DESIGN PARAMETERS

Controller parameters directly related to stability or steady state convergence (the first priority of control system design) are mostly determined when following the algorithmic design procedure. Other controller parameters, which have connection with alternative performance indicators, are customizable. Analytical relationship between those performance indices and the customizable parameters is usually very complex or not clear. Therefore, determination of those customizable parameters poses a challenge when performance requirements apart from steady state response are also critical. In this and next subsection, we will investigate influence of various controller parameters on the performance metrics proposed previously.

For this study, the number of fuzzy rules (i.e., M) is set to six. The Gaussian membership function $\mu_{F_i^l}$ in (14) can be expressed as

$$\mu_{F_i^l}(x_i) = \exp\left(-\frac{(x_i - c_l)^2}{2w_l^2}\right), \tag{34}$$

where c_l and w_l are often called the center and RMS width (i.e., standard deviation) of the membership function, which can be adopted as design parameters if their impact on aforementioned performance metrics can be justified. A total of twenty-four design parameters are available if the center and width of the membership functions for both $\boldsymbol{\xi}_f(\boldsymbol{x})$ and $\boldsymbol{\xi}_g(\boldsymbol{x})$ are taken into consideration. The influence of varying the parameters (i.e., range of center distribution and width) of the Gaussian membership function in $\boldsymbol{\xi}_f(\boldsymbol{x})$ on performance metrics is studied first (parameters in $\boldsymbol{\xi}_g(\boldsymbol{x})$ and others are kept at certain nominal values). The results are summarized in Table 2. It is concluded that both sets of parameters impact the performance metrics. Specifically, for the same range of center distribution, the RMSE, the voltage ripple, and the transient efficiency degrade as the width of the membership function increase, whereas the peak load current is barely affected. For the same width, the RMSE and the transient efficiency degrade as the range of center distribution widens, whereas the voltage ripple decreases and the peak load current is barely affected. Similar trend can be observed when varying the parameters in $\boldsymbol{\xi}_g(\boldsymbol{x})$ (parameters in $\boldsymbol{\xi}_f(\boldsymbol{x})$ and others are kept at certain nominal values).

Next, the influence of varying the parameters within the control law (k_1 and k_2 in $\boldsymbol{k}$ and $\boldsymbol{s}$) and the adaptation law (γ_f and γ_g in (19)) on performance metrics are investigated (parameters in $\boldsymbol{\xi}_f(\boldsymbol{x})$ and $\boldsymbol{\xi}_g(\boldsymbol{x})$ are kept at certain nominal values). The results are summarized in Table 3 and Table 4. It is concluded that both sets of parameters also impact the performance metrics. As shown in Table 3, as k_1 increases with other parameters fixed, both the RMSE and the voltage ripple reduce and the transient efficiency improves, but the peak load current deteriorates. When k_2 increases with other parameters fixed, the RMSE degrades gradually and the peak load current decreases whereas the voltage ripple and the transient efficiency are barely affected. As shown in Table 4, both γ_f and γ_g affect the performance metrics analogously. When both parameters increase, the RMSE and the voltage ripple reduce gradually, the transient efficiency improves, and the peak load current is hardly affected.

IV. MANY-OBJECTIVE GLOBAL OPTIMIZATION

The key elements in formulating an optimization problem are selection of a set of decision variables (design parameters) and objective functions (performance metrics). It is important to only include in the formulation the decision variables that certainly influence the objective functions. It is also useful to understand whether the adopted objective functions are conflicting or consonant. In the previous section, we identify

TABLE 2. Impact of the width (w) and range of center distribution ([0,20], [0,30], [0,60]) of the membership function in $\xi_f(x)$ on performance metrics of the converter.

w	RMSE (V)	Voltage ripple (V)	Peak load current (A)	Transient efficiency (%)
10	6.09	0.0037	30.54	58.8
	6.35	0.0027	30.56	58.7
	13.14	0.0005	30.94	39.7
15	7.2	0.8643	30.46	56.8
	7.21	0.8006	30.44	56.5
	15.12	0.0346	30.89	42.7
20	8.07	1.9099	30.41	55.5
	8.02	1.4215	30.42	55.0
	13.60	0.0011	30.84	45.6
25	8.73	2.8228	30.36	54.6
	8.65	2.4612	30.36	54.0
	12.84	0.0157	30.83	46.9
30	9.23	3.1189	30.34	53.8
	9.16	2.9407	30.34	53.7
	12.62	0.0165	30.80	47.4
35	9.62	3.4537	30.35	52.6
	9.57	3.4221	30.34	52.1
	12.63	0.0154	30.81	47.3
40	9.93	3.6261	30.35	52.4
	9.87	3.5871	30.35	52.2
	12.72	0.0157	30.78	47.2
45	10.16	3.6752	30.35	51.9
	10.12	3.5900	30.35	51.6
	12.84	0.0313	30.78	46.9
50	10.35	3.7590	30.34	51.3
	10.32	3.6356	30.34	51.2
	12.96	0.0148	30.75	46.6
55	10.5	3.9026	30.34	50.7
	10.46	3.8027	30.34	50.2
	13.05	0.0140	30.75	46.5
60	10.6	4.3607	30.34	50.5
	10.58	4.2325	30.34	50.1
	13.14	0.049	30.74	46.3

and define a set of performance metrics: RMSE, voltage ripple, switching peak load current, and transient efficiency. We also determine three groups of decision variables: centers (c_l) and widths (w_l) of the fuzzy membership functions in $\boldsymbol{\xi}_f(\boldsymbol{x})$ and $\boldsymbol{\xi}_g(\boldsymbol{x})$, k_1 and k_2 in the control law, and γ_f and γ_g in parametric adaptation law. Define the decision variable

$$\begin{aligned}\boldsymbol{p} = [&c_{1f}, w_{1f}, c_{2f}, w_{2f}, c_{3f}, w_{3f}, c_{4f}, w_{4f}, c_{5f}, w_{5f}, c_{6f},\\ &w_{6f}, c_{1g}, w_{1g}, c_{2g}, w_{2g}, c_{3g}, w_{3g}, c_{4g}, w_{4g}, c_{5g},\\ &w_{5g}, c_{6g}, w_{6g}, k_1, k_2, \gamma_f, \gamma_g],\end{aligned} \tag{35}$$

TABLE 3. Impact of varying k_1 and k_2 in the control law on performance metrics of the converter.

k_1 and k_2	RMSE (V)	Voltage ripple (V)	Peak load current (A)	Transient efficiency (%)
5000	9.41	0.052	16.98	55.94
	6.95	0.019	35.45	57.81
6000	8.92	0.045	19.35	56.24
	6.98	0.019	34.61	57.60
7000	8.43	0.038	22.28	56.56
	7.01	0.019	33.74	57.72
8000	7.966	0.032	25.46	56.93
	7.03	0.019	32.91	57.71
9000	7.501	0.025	28.28	57.24
	7.06	0.020	32.01	57.63
10000	7.093	0.020	31.26	57.63
	7.09	0.020	31.26	57.61
11000	6.757	0.016	33.89	57.94
	7.11	0.021	30.04	57.67
12000	6.504	0.012	36.41	58.3
	7.14	0.020	29.78	57.59
13000	6.32	0.010	38.60	58.3
	7.17	0.021	29.07	57.70
14000	6.15	0.008	40.23	58.5
	7.19	0.021	28.36	57.67
15000	6.03	0.007	41.42	58.4
	7.23	0.021	27.76	57.40

where subscripts f and g are added to further denote the association of c_l and w_l with $\boldsymbol{\xi}_f(\boldsymbol{x})$ and $\boldsymbol{\xi}_g(\boldsymbol{x})$, respectively. This section will proceed with formulating a many-objective optimization problem, which is stated formally as

$$\text{minimize } \boldsymbol{\phi}(\boldsymbol{p}) = \begin{bmatrix} \text{RMSE} & V_{ripple} & i_{L,\max} & -E_f \end{bmatrix}^T, \tag{36}$$

subject to

$$\begin{cases} c_{\min,f} \le c_{1f}, c_{2f}, c_{3f}, c_{4f}, c_{5f}, c_{6f} \le c_{\max,f}, \\ c_{\min,g} \le c_{1g}, c_{2g}, c_{3g}, c_{4g}, c_{5g}, c_{6g} \le c_{\max,g}, \\ w_{\min,f} \le w_{1f}, w_{2f}, w_{3f}, w_{4f}, w_{5f}, w_{6f} \le w_{\max,f}, \\ w_{\min,g} \le w_{1g}, w_{2g}, w_{3g}, w_{4g}, w_{5g}, w_{6g} \le w_{\max,g}, \\ k_{\min} \le k_1, k_2 \le k_{\max}, \gamma_{\min} \le \gamma_f, \gamma_g \le \gamma_{\max}, \end{cases} \tag{37}$$

where $\boldsymbol{\phi}(\boldsymbol{p})$ is a vector of objective functions, $c_{\min,f}$, $c_{\max,f}$, $c_{\min,g}$, $c_{\max,g}$, $w_{\min,f}$, $w_{\max,f}$, $w_{\min,g}$, $w_{\max,g}$, $k_{\min}$, $k_{\max}$, $\gamma_{\min}$, and $\gamma_{\max}$ are lower and upper bounds for the decision variables. The bounds on the decision variables define a decision or search space for the problem. Setting reasonable bounds can prevent the optimization algorithms from settling on impractical solutions (e.g., large values, zeros, negative values, and so on). Note that the minus sign on E_f indicates that this objective function is to be maximized. Two multi-objective algorithms, i.e., particle swarm optimization and bat optimization, are utilized to search the solutions. Both

TABLE 4. Impact of varying γ_f and γ_g in the parametric adaptation law on performance metrics of the converter.

γ_f and γ_g	RMSE (V)	Voltage ripple (V)	Peak load current (A)	Transient efficiency (%)
5000	9.09	0.110	30.97	53.96
	7.33	0.03	31.23	56.94
6000	8.54	0.059	30.98	54.87
	7.28	0.03	31.25	57.00
7000	8.08	0.039	31.03	55.66
	7.23	0.026	31.23	57.21
8000	7.69	0.029	31.09	56.61
	7.18	0.024	31.24	57.38
9000	7.36	0.024	31.14	57.22
	7.13	0.021	31.26	57.5
10000	7.09	0.024	31.26	57.63
	7.09	0.020	31.26	57.6
11000	6.838	0.017	31.36	58.11
	7.04	0.019	31.28	57.8
12000	6.619	0.014	31.40	58.44
	7.00	0.018	31.28	57.9
13000	6.42	0.012	31.42	58.69
	6.96	0.017	31.27	58.08
14000	6.24	0.01	31.48	59.1
	6.92	0.0161	31.31	58.18
15000	6.07	0.009	31.46	59.3
	6.89	0.0163	31.32	58.3

are swarm-based algorithms, by which they deploy a set of decision variables (i.e., particles or bats) into the search space and modify them based on certain rules. During the search process, the best-so-far decision variables will be tracked and recorded for subsequent determination of the optimal solution. Moreover, originally both algorithms are only applicable to single objective optimization. To extend their usage to many-objective optimization, both algorithms require modification and encompass the concept of Pareto solutions.

A. PARETO FRONT

Multi-objective function assigns to each decision variable a multi-objective vector function value in the objective function space. Instead of decision variable space, for multi-objective problems, we are usually more interested in the objective space and there is no natural ordering in this space. A solution $\boldsymbol{p}_1$ dominates $\boldsymbol{p}_2$ if the following two conditions are satisfied (n_ϕ is the number of objectives)

$$\begin{cases} \phi_i\left(\boldsymbol{p}_1\right) \leq \phi_i\left(\boldsymbol{p}_2\right), & \text{for } i = 1, 2, \ldots, n_\phi \\ \phi_j\left(\boldsymbol{p}_1\right) < \phi_j\left(\boldsymbol{p}_2\right), & \text{for at least one } j \in \left\{1, 2, \ldots, n_\phi\right\} \end{cases} \tag{38}$$

Hence, a solution is Pareto optimal, or nondominated, if there exists no other candidate solution that decreases some objectives without simultaneously increasing at least one other objective. The set of Pareto optimizers is called Pareto front. Computationally, the Pareto front is updated per iteration once non-dominated solutions are obtained during the search. Specifically, the newly acquired non-dominated solutions at each iteration are stored in an external archive of limited size. A scheme proposed in [41] may be utilized to decide whether a new solution enters the archive or a solution in the archive needs to be removed (i.e., update the Pareto front).

This study incorporated the method proposed by [37], [38]. An adaptive grid is utilized to uniformly spread the non-dominated solution along the Pareto front. The adaptive grid divides the objective space into hypercubes. Each hypercube is a bin that contains certain number of non-dominated solutions. When the external archive is full and a new non-dominated solution arrives, a solution in the most clustered hypercube is randomly selected and removed from the archive. To select a global best solution from the current Pareto front, each non-empty hypercube is assigned with a probability inversely proportional to the number of non-dominated solutions it holds. Then, a hypercube is chosen by employing roulette-wheel selection. From this hypercube, the global best may be selected randomly. Note that this will guide the search towards the area with less density of non-dominated solutions. As for the personal best, at first it is equal to the initial position of each particle or bat. At each iteration, the new position of a particle or bat and its current personal best are compared. If one dominates the other, either the current personal best is kept or it is replaced by the new position. If neither of them is dominated by the other, a random selection is made.

B. PARTICAL SWARM OPTIMIZATION

Particle swarm optimization (PSO) is a population-based stochastic optimization technique which shares many similarities with evolutionary algorithms. PSO is initialized with a population of random solutions, i.e., particles. Each particle is configured with velocity, position, cognitive and social traits, and personal experience history of fitness values. Each particle flies through the search space, i.e., updates its position, based on three information: velocity inertia, best personal fitness, best group fitness. To apply PSO to the formulated many-objective optimization problem, the selection and adaptive grid schemes introduced previously are adopted. At the beginning of the optimization, the particles are randomly initialized in a given space satisfying (37). The fitness of each particle is evaluated based on the performance metrics defined previously. An initial set of nondominated solutions can be determined using the scheme proposed in [41] and stored in an external archive. The particles update their positions and velocities by

$$\begin{cases} \boldsymbol{v}_i^{k+1} = \omega \boldsymbol{v}_i^k + c_1 \boldsymbol{r}_i^k \circ (\boldsymbol{p}_{i,\text{best}}^k - \boldsymbol{p}_i^k) + c_2 \boldsymbol{s}_i^k \circ (\boldsymbol{p}_{\text{best}}^k - \boldsymbol{p}_i^k), \\ \boldsymbol{p}_i^{k+1} = \boldsymbol{p}_i^k + \boldsymbol{v}_i^{k+1}, \end{cases} \tag{39}$$

where $\circ$ is Schur product, $\boldsymbol{v}_i^k$ and $\boldsymbol{p}_i^k$ are the velocity and position of particle i, respectively, at iteration k. Besides, ω is an inertial constant, c_1 and c_2 are cognitive and social constants, $\boldsymbol{r}_i^k$ and $\boldsymbol{s}_i^k$ are vectors of random numbers in (0,1). At each iteration, the personal best $\boldsymbol{p}_{i,\text{best}}^k$ and the global best $\boldsymbol{p}_{\text{best}}^k$ are determined by the aforementioned approach. The algorithm (including pseudo codes) is summarized as follows:

initialization ($k = 0$)
(1) Determine the numbers of particles and iterations.
(2) Initialize the position and the velocity of each particle.
(3) Initialize an external archive of certain size for storing Pareto solutions. This archive also stores the personal best of each particle.
(4) Evaluate the fitness of each particle by (36).
(5) Determine the non-dominated solutions and store them in the external archive. Generate hypercubes of the search space and position the particles in these hypercubes based on their objective function values.
(6) Select the global best from the archive.
(7) Set the personal best of each particle to the corresponding initial position.
end initialization
while ($k = k + 1 \leq$ maximum number of iterations)
(1) Update the velocity and the position of each particle according to (39).
(2) If any decision variable within the position of a particle exceeds the bounds described by (37), it will take the value of the corresponding lower or upper bound.
(3) Evaluate the fitness of each particle by (36).
(4) Update the non-dominated solutions in the external archive and perform adaptive grid scheme.
(5) Select the global best from the archive.
(6) Update the personal best of each particle.
end while

C. BAT OPTIMIZATION

Bat optimization (BO) is inspired by the echolocation ability of microbats during foraging. The echolocation behavior is similar to an active sonar system which sends out loud sound pulses and listens to echoes. Utilizing this ability, the bats can proactively locate their prey, distinguish the type of the prey, and avoid obstacles in a complete darkness environment. BO is also initialized with a population of random solutions, i.e., bats. Each bat is configured with velocity, position, frequency of sound, loudness, and pulse emission rate. The selection and adaptive grid schemes introduced previously are also adopted to apply BO to the formulated many-objective optimization problem. The bats are randomly initialized in a given space, i.e. (37). The fitness of each bat is evaluated according to the performance metrics. An initial set of nondominated solutions can be determined using the scheme proposed in [41] and stored in an external archive. The bats update their positions and velocities by

$$\begin{cases} freq_i^k = freq_{i,\min} + \beta(freq_{i,\max} - freq_{i,\min}), \\ \boldsymbol{v}_i^{k+1} = \omega \boldsymbol{v}_i^k + freq_i^k(\boldsymbol{p}_i^k - \boldsymbol{p}_{\text{best}}^k), \\ \boldsymbol{p}_i^{k+1} = \boldsymbol{p}_i^k + \boldsymbol{v}_i^{k+1}, \end{cases} \tag{40}$$

where $freq_i^k$, $\boldsymbol{v}_i^k$, and $\boldsymbol{p}_i^k$ are the frequency, velocity, and position of bat i, respectively, at iteration k. $freq_{i,\min}$ and $freq_{i,\max}$ are the minimum and maximum frequency, β is a random number in (0,1), and ω plays the same role as the inertia constant in PSO. At each iteration, the global best $\boldsymbol{p}_{\text{best}}^k$ is determined by the aforementioned approach. Here we adopt several nomenclatures for PSO. Equation (40) is quite similar to (39). However, BO has one additional feature, i.e., local search or random walk, which may further improve the solutions. The local search is conducted by

$$\boldsymbol{p}_{i,\text{new}}^k = \boldsymbol{p}_{\text{best}} + \varepsilon \bar{A}^k, \tag{41}$$

where $\boldsymbol{p}_{\text{best}}$ is a solution selected among the current set of non-dominated solutions (different from $\boldsymbol{p}_{\text{best}}^k$), ε is a random number in $(-1,1)$, and $\bar{A}^k$ is the average of the loudness A_i^k for all bats at iteration k. $\boldsymbol{p}_{i,\text{new}}^k$ is the new position to replace $\boldsymbol{p}_i^k$. Note that there is a probability mechanism (depending on the loudness and the pulse emission rate) which determines whether the local search is carried out for each bat at each iteration. The loudness A_i^k and the pulse emission rate γ_i^k are updated by

$$A_i^{k+1} = \alpha A_i^k, \gamma_i^{k+1} = \gamma_i^0(1 - e^{-\gamma k}), \tag{42}$$

where α and γ are constants typically in (0,1), the initial emission rate γ_i^0 is any value in [0,1], and the initial loudness A_i^0 can be set in [1,2]. α is analogous to the cooling factor in simulated annealing, which influences the convergence rate of the algorithm. The algorithm (including pseudo codes) is summarized as follows:

initialization ($k = 0$)
(1) Determine the numbers of bats and iterations.
(2) Initialize the position, the velocity, the frequency, the loudness, and the pulse emission rate of each bat.
(3) Initialize an external archive of certain size for storing Pareto solutions.
(4) Evaluate the fitness of each particle by (36).
(5) Determine the non-dominated solutions and store them in the external archive. Generate hypercubes of the search space and position the particles in these hypercubes based on their objective function values.
(6) Select the global best from the archive.
end initialization
while ($k = k + 1 \leq$ maximum number of iterations)
(1) Update the frequency, the velocity, and the position of each bat according to (40).
(2) Perform a local search:
for (each bat i)
If (random number $> \gamma_i^k$)
Perform a local search according to (41).

TABLE 5. Specification of a laboratory PSPWM full bridge DC-DC power converter.

Parameters	Symbol	Value	Unit
Rated power	P_{rated}	850	Watts
Input DC voltage	v_i	160	Volts
Output DC voltage	v_o	50	Volts
Load resistance	R	3	Ω
Capacitance of rectification filter	C	940	μF
Inductance of rectification filter	L	300	μH
Leakage inductance	L_{lk}	20	μH
Parasitic capacitance	C_A, C_B, C_C, C_D	5	nF
Switching frequency	f_s	50	kHz

If (random number $< A_i^k$ and $\boldsymbol{p}_{i,\text{new}}^k$ is not dominated by $\boldsymbol{p}_{\text{best}}^k$) Set $\boldsymbol{p}_i^k$ to $\boldsymbol{p}_{i,\text{new}}^k$.
end if
end if
end for

(3) If any decision variable within the position of a particle exceeds the bounds described by (37), it will take the value of the corresponding lower or upper bound. Also, the sign of the respective decision variable within the velocity is reversed (i.e., positive to negative and vice versa).
(4) Evaluate the fitness of each particle by (36).
(5) Update the non-dominated solutions in the external archive and perform adaptive grid scheme.
(6) Select the global best from the archive.

end while

V. PARAMETRIC OPTIMIZATION OF THE CONTROLLER

As described in Section II, design and synthesis of adaptive fuzzy with sliding model controller is based on a reduced-order model with specified uncertainty bounds. A computing framework is proposed in this section for parametric optimization of the controller. In order to have sophisticated dynamics in the output response for realistic evaluation of the performance metrics defined previously, a sophisticated model is required for the simulation framework. Specifically, the controller is connected with the elaborate computational model [40] (instead of the reduced-order model) in subsequent numerical simulation for analysis of the overall control system. Besides the simulation results having better practicability, this also reduces hardware design effort and saves experiment cost.

A. SIMULATION SETUP

A computational platform based on MATLAB/Simulink environment is established for parametric optimization of the controller (see Fig. 3). The mathematical model of the PSPWM full bridge DC-DC power converter along with the adaptive fuzzy with sliding mode controller is realized and implemented in Simulink. The specification of a laboratory power converter to be used for subsequent experiment is detailed in Table 5. The many-objective optimization algorithm (PSO or BO) is implemented in MATLAB. For each iteration, an updated set of design parameters is generated by the optimization algorithm (in MATLAB), and given to the controller of the adaptive fuzzy with sliding mode control system for numerical simulation (in Simulink). After each simulation is completed, performance metrics are evaluated and provided to the optimization algorithm for further actions, e.g., updating the design parameters and the Pareto front.

For synthesis of the adaptive fuzzy with sliding mode controller, apart from design parameters, there are other parameters which are relevant to stability, e.g., θ_{Lfi}, θ_{fi}^U, θ_{Lgi}, θ_{gi}^U, d_f, d_g, k_s, γ, μ, etc. It is advisable to 'manually' determine the values of those parameters. Likewise, there are user parameters within PSO and BO algorithms, which need to be determined beforehand., e.g., upper and lower bounds for design parameters, number of iteration, number of particles or bats, number of hypercubes, weights for correction terms to velocity, maximum and minimum frequencies of bats, maximum/minimum loudness of bats, etc. Some of those parameters might influence the convergence property. For this study, the upper and lower bounds for centers are set to 300 and 0, respectively. The upper and lower bounds for widths are set to 80 and 1, respectively. The upper and lower bounds for k_1, k_2, γ_f and γ_g are set to 50,000 and 10, respectively. The numbers of iteration, particles/bats, and the size of external archive are set to 50, 10, and 10, respectively. Other parameters are set to typical values provided in the literature.

Note that several sophisticated dynamics, which might affect performance metrics, are included in the numerical model of PSPWM full bridge DC-DC power converter: PWM driver, phase-shift switching logic, and ZVS delay. In order to capture the above dynamics, the sampling frequency needs to be set to a much higher value than, for example, the PWM frequency (50 kHz). Therefore, a sampling frequency of 10 MHz is used for simulation. On a laboratory computer with Intel Core i7 (9700) 3.4 GHz CPU and 16GB RAM running MATLAB/Simulink R2020b, it takes approximately 20 minutes to complete a 2.5 seconds simulation for the adaptive fuzzy with sliding mode control system. Execution time of the optimization algorithm, performance metric evaluation, and Pareto front update also adds to the simulation time. Therefore, a full cycle of optimization run takes around seven days to complete. In the Conclusion section, methods or techniques for speeding up the simulation will be discussed.

B. PARETO SOLUTIONS

The many-objective optimization problem formulated by (36)and (37) is numerically solved based on the computational framework proposed previously. Both PSO and BO algorithms are utilized to produce separate Pareto fronts for comparative study. Recall that at each iteration the optimization algorithm will generate a set of feasible design

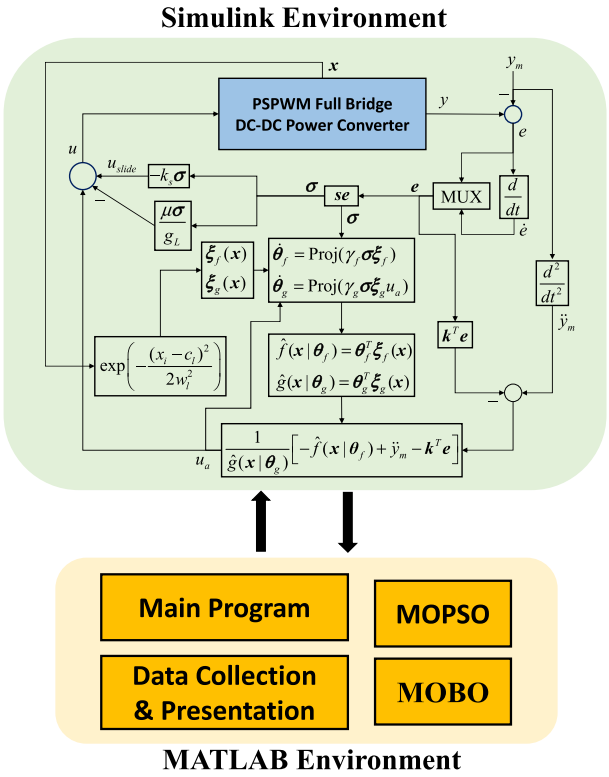

FIGURE 3. A computational platform based on MATLAB/Simulink environment for parametric optimization of the controller.

TABLE 6. A set of candidate Pareto solutions obtained amid BO.

Non-dominated solutions	RMSE (V)	Voltage ripple (V)	Peak load current (A)	Transient efficiency (%)
# 1	2.2	0.0028	43	63.22
# 2	4.6153	0.0165	30.5	61.46
# 3	4.578	0.0038	20	62.19
# 4	3.2196	0.3518	32.3	62.74
# 5	2.1994	0.0028	43	63.19
# 6	2.2276	0.0027	42.8	63.2
# 7	2.207	0.0026	41.3	63.21
# 8	2.278	0.0024	43.2	63.14
# 9	2.3028	0.0017	43.4	63.08
# 10	2.8358	0.0093	42.09	60.6

parameters. Then the selection mechanism described previously is applied to extract candidate non-dominated or Pareto solutions from this set of design parameters. Note that the adopted selection mechanism can only approximate the 'true' Pareto front. The accuracy depends on factors such as number of particles, number of iterations, initial positions of particles, etc. A set of candidate Pareto solutions during BO is listed in Table 6. As can be verified that those solutions all satisfy (38) for the definition of non-dominated solutions.

The Pareto fronts are acquired after the specified number of iterations. Since there are four performance metrics, it is not possible to demonstrate the Pareto fronts in four-dimensional space. Alternatively, "projected" two-dimensional metric-versus-metric presentation is adopted and three representative results are shown in Fig. 4. Specifically, Fig. 4(a) shows the "projected" two-dimensional Pareto fronts for RSME versus voltage ripple, Fig. 4(b) shows the Pareto fronts for transient efficiency versus peak load current, and Fig. 4(c) shows the Pareto front for RSME versus peak load current. Recall that the size of the external archive for storing Pareto solutions is set to ten. As can be seen, BO performs better than PSO in locating the Pareto fronts for RSME versus voltage ripple and RSME versus peak load current. Nevertheless, PSO performs better in locating the Pareto front for transient efficiency versus peak load current. An unoptimized case (with a set of parameters obtained empirically) is also marked on each figure for comparison. All performance metrics corresponding to the unoptimized case can be seen to be dominated by those obtained using MOBO. They are only 'partially' dominated by those obtained using MOPSO, which indicates that the Pareto front associated with MOPSO can be further improved, e.g., more iterations. The unoptimized case actually almost lies on the projected Pareto front (RMSE versus voltage ripple) located by MOBO. Overall, both the MOPSO and MOBO identify various sets of design parameters, with which the corresponding controllers can noticeably improve the performance of the PSPWM full bridge DC-DC power converter. Note, however, that the conflicting nature of the performance metrics are also observed from Fig. 4, i.e., having one metric minimized for a solution comes at a price of having the other metric maximized and vice versa. Quantitative improvement is summarized in Table 7. The adaptive fuzzy with sliding mode controller using one of the Pareto solutions acquired from the MOPSO can reduce the voltage ripple by 55.81%, reduce the peak load current by 21.73%, and improve the transient efficiency by 2.59% despite RMSE being sacrificed. Similarly, the controller using one of the Pareto solutions acquired from the MOBO can reduce the RMSE by 17.00%, reduce the voltage ripple by 31.40%, reduce the peak load current by 29.73%, and improve the transient efficiency by 1.79%. The current and voltage responses corresponding to the unoptimized case and two of the Pareto solutions (which produce minimum or maximum performance metrics) are shown in Fig. 5. The design parameters corresponding to Fig. 5(b), rounded to the nearest integers, are $k_1 = 25, 134$, $k_2 = 40, 596$, $\gamma_f = 20, 071$ and $\gamma_g = 25, 408$, and the design parameters corresponding to Fig. 5(c) are $k_1 = 7, 533$, $k_2 = 7, 557$, $\gamma_f = 10, 522$ and $\gamma_g = 25, 673$. The corresponding fuzzy membership functions are given in Fig. 6.

The Pareto solutions acquired correspond to a set of controllers for the PSPWM full bridge DC-DC power converter. One characteristic of any two controllers from this set is that a gain in a performance metric from one controller to the other happens only because of a sacrifice in at least on other performance metric. This trade-off property raises a question concerning how a practitioner makes a final choice among the non-dominated controllers. If the decision

TABLE 7. Quantitative improvement of the PSPWM full bridge DC-DC power converter using the Pareto optimal controllers.

	RMSE (V)	RMSE improvement (%)	Voltage ripple (V)	Voltage ripple improvement (%)	Peak load current (A)	Peak load current improvement (%)	Transient efficiency (%)	Transient efficiency improvement (%)
Unoptimized	3.417		0.0086		37.00		60.380	
MOPSO	3.703	-8.37	**0.0038**	**55.81**	28.96	21.73	**62.970**	**2.59**
MOBO	**2.836**	**17.00**	0.0059	31.40	**26.00**	**29.73**	62.170	1.79

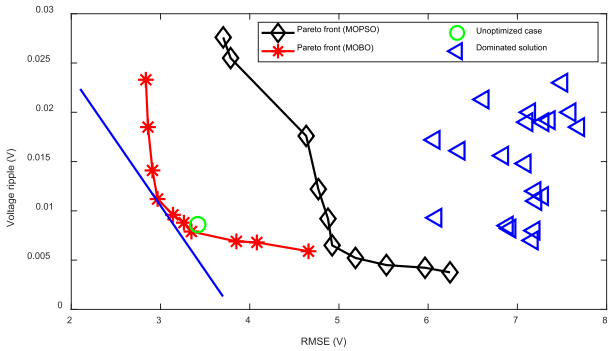

(a) RSME versus voltage ripple.

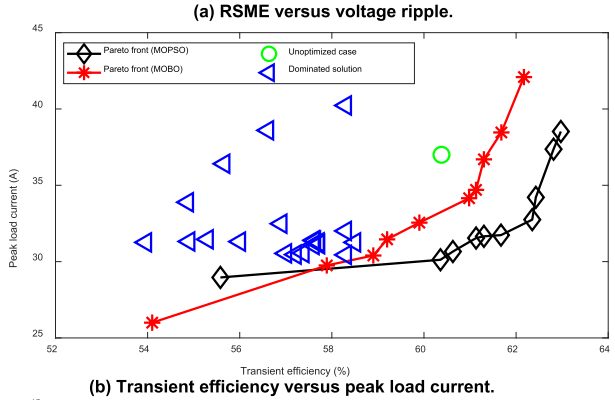

(b) Transient efficiency versus peak load current.

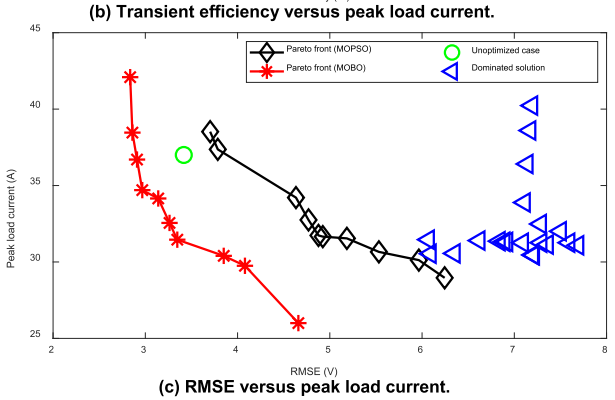

(c) RMSE versus peak load current.

FIGURE 4. Projected two-dimensional Pareto fronts.

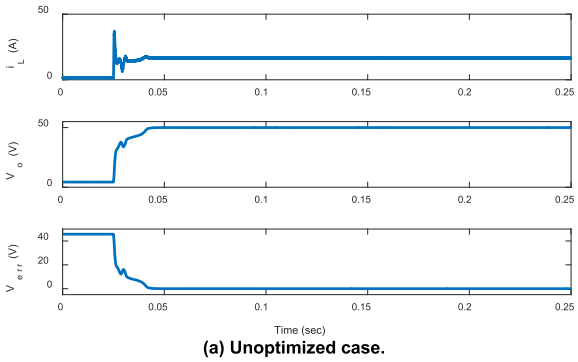

(a) Unoptimized case.

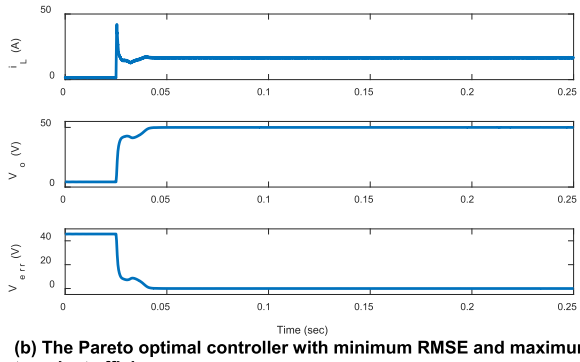

(b) The Pareto optimal controller with minimum RMSE and maximum transient efficiency.

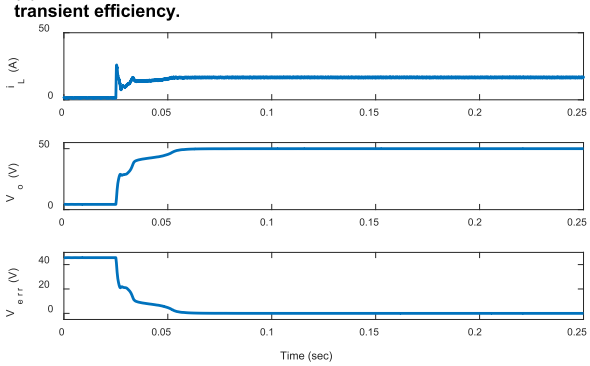

(c) The Pareto optimal controller with minimum ripple voltage and minimum peak load current.

FIGURE 5. The current and voltage responses corresponding to the unoptimized case and two of the Pareto solutions.

maker has additional information regarding the preference of each performance metric, he/she may create a hyperplane (i.e., a single-objective function) by forming a weighted sum of the performance metrics with the weight indicating the importance. Locating the approximate tangent point of this hyperplane with the Pareto front will provide the decision maker with an optimal solution. An example is illustrated in Fig. 4(a). Suppose that only trade-off between RMSE and voltage ripple needs to be made. The red curve in the figure is the Pareto front obtained using the MOBO algorithm. The blue line represents a single-objective function by forming the weighted sum or linear combination of these two performance metrics. The approximate tangent point is around RMSE $=$ 2.964 and $V_{ripple} = 0.011$. When there is no 'actual' tangent point, adjacent data point may be identified and used instead.

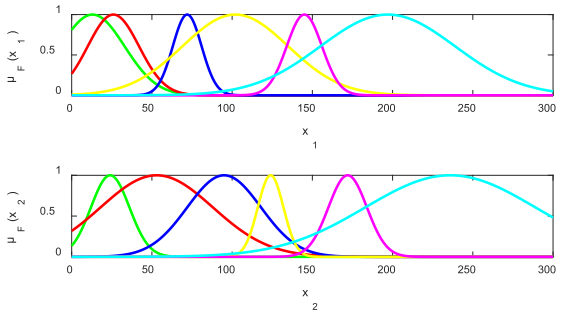

(a) The one with minimum RMSE and maximum transient efficiency.

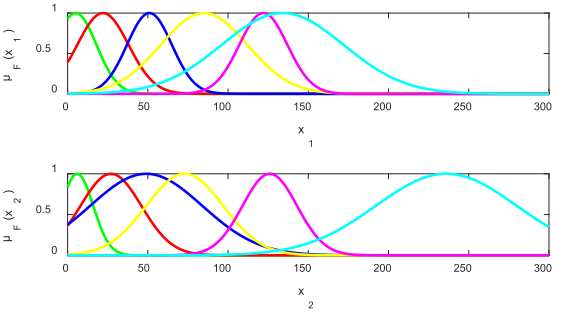

(b) The one with minimum ripple voltage and minimum peak load current.

FIGURE 6. The fuzzy membership functions (with design parameters of centers and widths) corresponding to two of the Pareto optimal controllers.

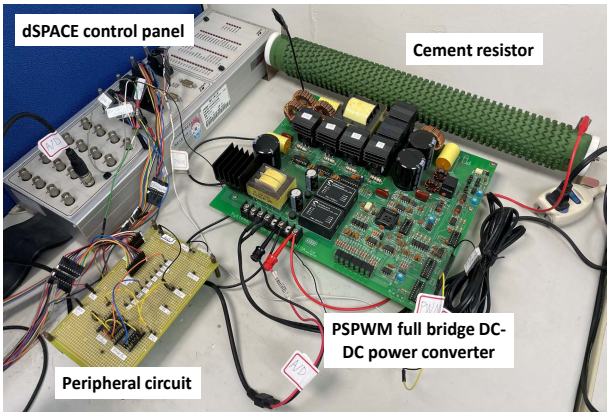

FIGURE 7. An experimental platform with dSPACE controller board.

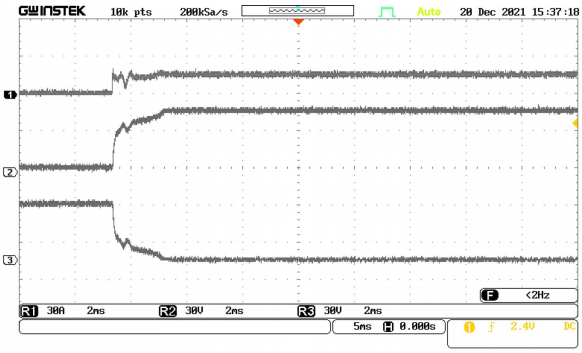

(a) Unoptimized case

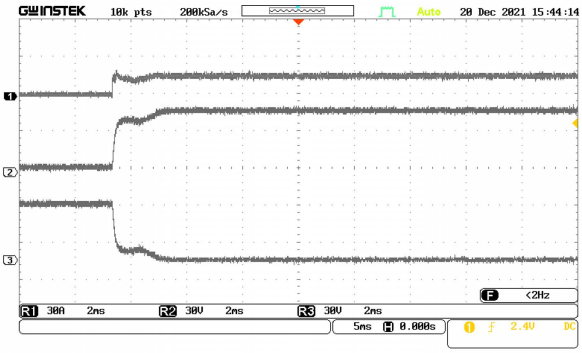

(b) The Pareto optimal controller with minimum RMSE and maximum transient efficiency.

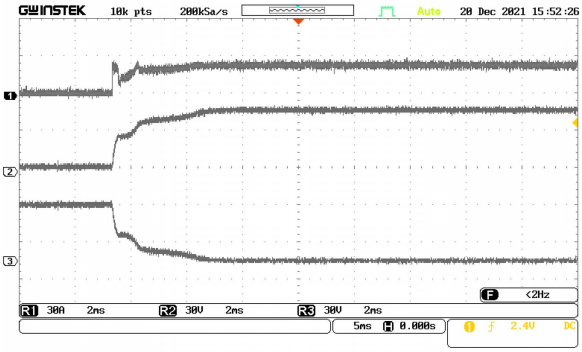

(c) The Pareto optimal controller with minimum ripple voltage and minimum peak load current.

FIGURE 8. The current and voltage responses corresponding to the unoptimized case and two of the Pareto solutions (signal 1: load current; signal 2: voltage output; signal 3: voltage error).

VI. EXPERIMENTAL RESULTS

An experimental platform is utilized to further justify the proposed parametric optimization scheme for controller synthesis. This platform, as shown in Fig. 7, mainly consists of a PSPWM full bridge DC-DC power converter (as described in [42]) and a dSPACE DS1104 controller board (with peripherals and software) for rapid control prototyping. The power converter allows voltage output ranging from 0 V to 50 V. The controller board supports models created within Simulink environment and provides efficient method to develop and test new control strategies quickly without manual programming. More explicitly, to adopt the adaptive fuzzy with sliding mode control system developed previously (within Simulink environment) and implement it on the experimental platform, certain alterations are essential: (1) The model for the PSPWM full bridge DC-DC power converter is removed from the control system and replaced by a physical converter (see Fig. 7). Some I/O blocks are added to the model serving as software and hardware interface; (2) Peripheral circuits (e.g., voltage and current sensors and transducers) connecting the power convert to the controller board are made; (3) The model for the adaptive fuzzy with sliding model controller requires certain modification (e.g., replacing fuzzy membership function with its numerical approximation) to ensure compatibility with the software for the controller board.

The current and voltage responses for the converter with a typical set of unoptimized controller parameters (formerly used for Fig. 5(a)) are shown in Fig. 8(a). The current and voltage responses corresponding to the Pareto solutions, which produce minimum or maximum performance metrics

(as formerly shown in Fig. 5(b)(c)), are shown in Fig. 8(b)(c). As expected or predicted by the simulation results, the responses with optimized controller parameters demonstrate significant improvement when compared to those of the unoptimized case. Specifically, the output voltage in Fig. 8(b) is closer to the reference output, resulting in smaller RMSE. The transient efficiency is also maximized in this case. The voltage ripple in Fig. 8(c) is less than that for the unoptimized case and the peak load current is also minimized. Overall, the experimental results suggest that the proposed parametric optimization scheme achieves 29.62, 25.00, 30.16, and 1.69 percentage of improvement in RMSE, ripple voltage, peak load current, and transient efficiency, respectively. Note that the amplitude of the peak load current for the power converter of the experimental platform is less than that for the simulation model. This may due to the snubber circuit composed by the parasitic parameters of switches or other electric components in the hardware-implemented power converter.

VII. CONCLUSION AND FUTURE WORK

A parametric optimization framework amid the synthesis of a robust adaptive fuzzy controller for a class of switching power converters applicable to renewable energy systems is presented in this paper. Four performance metrics essential to the practical needs of renewable energy application are suggested, and the corresponding many-objective optimization problem is formulated. MOPSO and MOBO are employed to numerically solve the problem and obtain a set of Pareto optimal controllers. Both simulation and experiment validate that those optimal controllers significantly improve the performance metrics of the control system.

Although the proposed optimization framework is only demonstrated for one set of operating point, i.e., input and output. To obtain the Pareto optimal controllers for other operating points, simply repeat the procedure described. Therefore, the decision maker will have numerous sets of optimal controllers with each corresponding to an operating point. Note that individual performance metric can have different emphasis with respect to different operating point, i.e., various sets of weights can be designated to performance metrics for different operating points. Afterwards, the weighted sum method, e.g., Fig. 4(a), can be used to choose the most appropriate controller for each operating point. It is also feasible to apply the proposed method to the scenario where parametric optimization is performed over a set of operating points, which will become an expansion of this work. However, it would be suspected that controllers obtained from such greedy strategy can have superior performance.

Another issue is regarding the lengthy off-line simulation time required utilizing the proposed computational platform for parametric optimization. Immediate solutions might be to upgrade the computing hardware or consider parallel computing using multiple computers (and merge the results). The major bottleneck of time is mainly due to the elaborate model incorporating the dynamics of the phase-shift PWM. Under the circumstance that the impact of the PWM dynamics on the performance metrics is negligible, the model can be further simplified, which should significantly reduce the time of simulation. Moreover, parts of the performance metrics adopted for this work, e.g., RMSE and efficiency, may be revised so that they are evaluated at each iteration or every few iterations. The controller parameters may be updated at the same pace. Therefore, machine learning algorithm such as reinforcement learning may be considered to perform on-line parametric optimization, which will require only one simulation run. Note, however, that not all performance metrics can be assessed immediately amid numerical simulation. This will be another future expansion of this work.

ACKNOWLEDGMENT

The author would like to thank Bang-Qi Liu (Taiwan Power Company) for accumulating data in this study. He would also like to thank Dr. Cong-Sheng Huang (North Carolina State University) for assisting with an earlier version of the manuscript.

REFERENCES

[1] A. I. S. Senthilkumar, D. Biswas, and M. Kaliamoorthy, "Dynamic power management system employing a single-stage power converter for standalone solar PV applications," *IEEE Trans. Power Electron.*, vol. 33, no. 12, pp. 10352–10362, Dec. 2018, doi: 10.1109/TPEL.2018.2804658.

[2] A. Hussain, V.-H. Bui, and H.-M. Kim, "Optimal sizing of battery energy storage system in a fast EV charging station considering power outages," *IEEE Trans. Transp. Electrific.*, vol. 6, no. 2, pp. 453–463, Jun. 2020, doi: 10.1109/TTE.2020.2980744.

[3] Q. Ouyang, G. Xu, H. Fang, and Z. Wang, "Fast charging control for battery packs with combined optimization of charger and equalizers," *IEEE Trans. Ind. Electron.*, vol. 68, no. 11, pp. 11076–11086, Nov. 2021, doi: 10.1109/TIE.2020.3029464.

[4] K. V. Raghavendra, K. Zeb, A. Muthusamy, and T. N. V. Krishna, "A comprehensive review of DC–DC converter topologies and modulation strategies with recent advances in solar photovoltaic systems," *Electronics*, vol. 9, no. 1, p. 31, 2020, doi: 10.3390/electronics9010031.

[5] S. A. Q. Mohammed and J. W. Jung, "A state-of-the-art review on soft-switching techniques for DC-DC, DC-AC, AC-DC, and AC-AC power converters," *IEEE Trans. Ind. Informat.*, vol. 17, no. 10, pp. 6569–6582, Oct. 2021, doi: 10.1109/TII.2021.3058218.

[6] W. Sima, D. Peng, M. Yang, P. Sun, B. Zou, and Z. Xiong, "Reversible wideband hybrid model of two-winding transformer including the core nonlinearity and EMTP implementation," *IEEE Trans. Ind. Electron.*, vol. 68, no. 4, pp. 3159–3169, Apr. 2021, doi: 10.1109/TIE.2020.2977544.

[7] A. Iovine, S. B. Siad, G. Damm, E. De Santis, and M. D. Di Benedetto, "Nonlinear control of a DC microgrid for the integration of photovoltaic panels," *IEEE Trans. Automat. Sci. Eng.*, vol. 14, no. 2, pp. 524–535, Apr. 2017, doi: 10.1109/TASE.2017.2662742.

[8] C.-C. Chen, C.-L. Chen, J.-X. Chang, and C.-F. Yang, "LPV gain-scheduling control for a phase-shifted PWM full-bridge soft switched converter," *IFAC Proc. Volumes*, vol. 47, no. 3, pp. 6135–6140, 2014, doi: 10.3182/20140824-6-ZA-1003.02377.

[9] W. Dong, S. Li, X. Fu, Z. Li, M. Fairbank, and Y. Gao, "Control of a buck DC/DC converter using approximate dynamic programming and artificial neural networks," *IEEE Trans. Circuits Syst. I, Reg. Papers*, vol. 68, no. 4, pp. 1760–1768, Apr. 2021, doi: 10.1109/TCSI.2021.3053468.

[10] E. M. Rocha, W. Barra, K. E. Lucas, R. L. P. Medeiros, and D. A. Vaca-Benavides, "Design and experimental assessment of a robust voltage control for DC-DC converters considering components parametric uncertainties," *IEEE Access*, vol. 8, pp. 109217–109231, 2020, doi: 10.1109/ACCESS.2020.2997014.

[11] M. Merai, M. W. Naouar, I. Slama-Belkhodja, and E. Monmasson, "An adaptive PI controller design for DC-link voltage control of single-phase grid-connected converters," *IEEE Trans. Ind. Electron.*, vol. 66, no. 8, pp. 6241–6249, Aug. 2019, doi: 10.1109/TIE.2018.2871796.

[12] K. Viji, A. Kumar, and R. Nagaraj, "Improved delta operator based discrete sliding mode fuzzy controller for buck converter," *Indian J. Sci. Technol.*, vol. 10, no. 25, pp. 1–11, 2017, doi: 10.17485/ijst/2017/v10i25/116507.
[13] B.-Q. Liu and C.-L. Chen, "Modeling and robust adaptive fuzzy control for servo layer control of a motor/gear subsystem," in *Proc. 14th IEEE Conf. Ind. Electron. Appl. (ICIEA)*, Jun. 2019, pp. 1835–1840, doi: 10.1109/ICIEA.2019.8834373.
[14] K.-C. Liu, C.-L. Chen, and C.-Y. Siao, "Modeling, analysis, and robust adaptive fuzzy control for a class of switching power converters," in *Proc. 12th IEEE Conf. Ind. Electron. Appl. (ICIEA)*, Jun. 2017, pp. 1149–1154, doi: 10.1109/ICIEA.2017.8283013.
[15] S. Tong, T. Wang, Y. Li, and B. Chen, "A combined backstepping and stochastic small-gain approach to robust adaptive fuzzy output feedback control," *IEEE Trans. Fuzzy Syst.*, vol. 21, no. 2, pp. 314–327, Apr. 2013, doi: 10.1109/TFUZZ.2012.2213260.
[16] T. Shaocheng, L. Changying, and L. Yongming, "Fuzzy adaptive observer backstepping control for MIMO nonlinear systems," *Fuzzy Sets Syst.*, vol. 160, no. 19, pp. 2755–2775, 2009, doi: 10.1016/j.fss.2009.03.008.
[17] S. Tong and Y. Li, "Observer-based fuzzy adaptive control for strict-feedback nonlinear systems," *Fuzzy Sets Syst.*, vol. 160, no. 12, pp. 1749–1764, 2009, doi: 10.1016/j.fss.2008.09.004.
[18] P. Sanjeevikumar, E. Ozsoy, V. Fedák, and F. Blaabjerg, "Development of sliding mode controller for a modified boost Ćuk converter configuration," *Energies*, vol. 10, no. 10, p. 1513, Sep. 2017, doi: 10.3390/en10101513.
[19] M. Elsisi, N. Bazmohammadi, J. M. Guerrero, and M. A. Ebrahim, "Energy management of controllable loads in multi-area power systems with wind power penetration based on new supervisor fuzzy nonlinear sliding mode control," *Energy*, vol. 221, Apr. 2021, Art. no. 119867, doi: 10.1016/j.energy.2021.119867.
[20] J. Guo, "Application of a novel adaptive sliding mode control method to the load frequency control," *Eur. J. Control*, vol. 57, pp. 172–178, Jan. 2021, doi: 10.1016/j.ejcon.2020.03.007.
[21] L. Yutao and W. Feng, "Optimization of bidirectional DC/DC converter for electric vehicles based on driving cycle," *J. Elect. Eng. Technol.*, vol. 12, no. 5, pp. 1934–1944, Jan. 2017, doi: 10.5370/JEET.2017.12.5.1934.
[22] S. H. Kang, D. Maksimović, and I. Cohen, "Efficiency optimization in digitally controlled flyback DC–DC converters over wide ranges of operating conditions," *IEEE Trans. Power Electron.*, vol. 27, no. 8, pp. 3734–3748, Aug. 2012, doi: 10.1109/TPEL.2012.2186590.
[23] K. Sabanci and S. Balci, "Development of an expression for the output voltage ripple of the DC-DC boost converter circuits by using particle swarm optimization algorithm," *Measurement*, vol. 158, Jul. 2020, Art. no. 107694, doi: 10.1016/j.measurement.2020.107694.
[24] U. Mumtahina and P. J. Wolfs, "Multimode optimization of the phase-shifted LLC series resonant converter," *IEEE Trans. Power Electron.*, vol. 33, no. 12, pp. 10478–10489, Dec. 2018, doi: 10.1109/TPEL.2018.2803741.
[25] A. Garcia-Bediaga, I. Villar, A. Rujas, L. Mir, and A. Rufer, "Multiobjective optimization of medium-frequency transformers for isolated soft-switching converters using a genetic algorithm," *IEEE Trans. Power Electron.*, vol. 32, no. 4, pp. 2995–3006, Apr. 2017, doi: 10.1109/TPEL.2016.2574499.
[26] R. S. Alishah, S. H. Hosseini, E. Babaei, and M. Sabahi, "Optimization assessment of a new extended multilevel converter topology," *IEEE Trans. Ind. Electron.*, vol. 64, no. 6, pp. 4530–4538, Jun. 2017, doi: 10.1109/TIE.2017.2669885.
[27] S. Banerjee, A. Ghosh, and N. Rana, "An improved interleaved boost converter with PSO-based optimal type-III controller," *IEEE J. Emerg. Sel. Topics Power Electron.*, vol. 5, no. 1, pp. 323–337, Mar. 2017, doi: 10.1109/JESTPE.2016.2608504.
[28] A. Divakar and J. Jacob, "Genetic algorithm based tuning of nonfragile and robust PI controller for PSFB DC-DC converter," in *Proc. Int. Conf. Commun. Electron. Syst. (ICCES)*, Jul. 2019, pp. 1846–1851, doi: 10.1109/ICCES45898.2019.9002210.
[29] J. B. L. Fermeiro, J. A. N. Pombo, M. R. A. Calado, and S. J. P. S. Mariano, "A new controller for DC-DC converters based on particle swarm optimization," *Appl. Soft Comput.*, vol. 52, pp. 418–434, Mar. 2017, doi: 10.1016/j.asoc.2016.10.025.
[30] A. Karaarslan, "The implementation of bee colony optimization algorithm to Sheppard–Taylor PFC converter," *IEEE Trans. Ind. Electron.*, vol. 60, no. 9, pp. 3711–3719, Sep. 2013, doi: 10.1109/TIE.2012.2204711.
[31] N. Priyadarshi, V. K. Ramachandaramurthy, S. Padmanaban, and F. Azam, "An ant colony optimized MPPT for standalone hybrid PV-wind power system with single Cuk converter," *Energies*, vol. 12, no. 1, p. 167, 2019.
[32] K. Durgadevi and R. Karthik, "Performance analysis of zeta converter using classical PID and fractional order PID controller," in *Proc. Int. Conf. Power, Energy, Control Transmiss. Syst. (ICPECTS)*, Feb. 2018, pp. 312–317, doi: 10.1109/ICPECTS.2018.8521573.
[33] S.-Y. Chen, B.-C. Yang, T.-A. Pu, C.-H. Chang, and R.-C. Lin, "Active current sharing of a parallel DC-DC converters system using bat algorithm optimized two-DOF PID control," *IEEE Access*, vol. 7, pp. 84757–84769, 2019, doi: 10.1109/ACCESS.2019.2925064.
[34] R. Suchithra, K. Ezhilsabareesh, and A. Samad, "Optimization based higher order sliding mode controller for efficiency improvement of a wave energy converter," *Energy*, vol. 187, Nov. 2019, Art. no. 116111, doi: 10.1016/j.energy.2019.116111.
[35] N. Hou, W. Song, Y. Li, Y. Zhu, and Y. Zhu, "A comprehensive optimization control of dual-active-bridge DC-DC converters based on unified-phase-shift and power-balancing scheme," *IEEE Trans. Power Electron.*, vol. 34, no. 1, pp. 826–839, Jan. 2019, doi: 10.1109/TPEL.2018.2813995.
[36] J. Knowles and D. Corne, "Properties of an adaptive archiving algorithm for storing nondominated vectors," *IEEE Trans. Evol. Comput.*, vol. 7, no. 2, pp. 100–116, Apr. 2003, doi: 10.1109/TEVC.2003.810755.
[37] C. A. C. Coello, G. T. Pulido, and M. S. Lechuga, "Handling multiple objectives with particle swarm optimization," *IEEE Trans. Evol. Comput.*, vol. 8, no. 3, pp. 256–279, Jun. 2004, doi: 10.1109/TEVC.2004.826067.
[38] N.-C. Yang and M.-D. Le, "Optimal design of passive power filters based on multi-objective bat algorithm and Pareto front," *Appl. Soft Comput.*, vol. 35, pp. 257–266, Oct. 2015, doi: 10.1016/j.asoc.2015.05.042.
[39] L. Li, G. P. Li, and L. Chang, "A many-objective particle swarm optimization with grid dominance ranking and clustering," *Appl. Soft Comput.*, vol. 96, Nov. 2020, Art. no. 106661, doi: 10.1016/j.asoc.2020.106661.
[40] C.-L. Chen, "Robust adaptive fuzzy control for a class of switching power converters," in *Modern Fuzzy Control Systems and Its Applications*. Rijeka, Croatia: InTech, 2017, p. 139.
[41] E. K. Chong and S. H. Zak, *An Introduction to Optimization*, 4th ed. Hoboken, NJ, USA: Wiley, 2013.
[42] C.-L. Chen and C.-S. Huang, "An efficient phase shift full bridge DC/DC converter with wide range voltage output: Design and hardware implementation," *J. Electr. Eng. Technol.*, pp. 1–12, Dec. 2021, doi: 10.1007/s42835-021-00970-8.

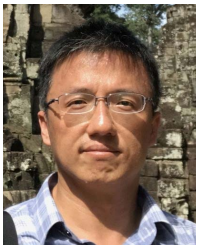

CHENG-LUN CHEN (Member, IEEE) received the B.S. and M.S. degrees in power mechanical engineering from the National Tsing Hua University, Hsinchu, Taiwan, in 1993 and 1995, respectively, and the Ph.D. degree in mechanical engineering (with a major in control) from Purdue University, West Lafayette, IN, USA, in 2003. He had been a Second Missile and Artillery Lieutenant for obligatory military service, from 1995 to 1997. He was a System Engineer at RPTI International Ltd., from 1997 to 1998. He worked as a Control Engineer for Lexmark International, Inc., from 2003 to 2004. He is currently an Associate Professor with the National Chung Hsing University, Taiwan. His research interests include robust control, repetitive and iterative learning control, motor drives and power converters, image quality enhancement, and applications of optimization algorithms. He was a recipient of the 2010 Outstanding Paper Award of the IEEE TRANSACTIONS ON CONTROL SYSTEMS TECHNOLOGY.